Journal of Atmospheric and Solar-Terrestrial Physics 167 (2018) 124–133

Contents lists available at ScienceDirect

Journal of Atmospheric and Solar-Terrestrial Physics

journal homepage: www.elsevier.com/locate/jastp

GPS-based PWV for precipitation forecasting and its application to a typhoon event

Qingzhi Zhao [a,*], Yibin Yao [b,c], Wanqiang Yao [a]

[a] College of Geomatics, Xi'an University of Science and Technology, Xi'an, China
[b] School of Geodesy and Geomatics, Wuhan University, Wuhan, China
[c] Key Laboratory of Geospace Environment and Geodesy, Ministry of Education, Wuhan University, Wuhan, China

ARTICLE INFO

Keywords:
GNSS
PWV
Precipitation forecasting
Least-square fitting method

ABSTRACT

The temporal variability of precipitable water vapour (PWV) derived from Global Navigation Satellite System (GNSS) observations can be used to forecast precipitation events. A number of case studies of precipitation events have been analysed in Zhejiang Province, and a forecasting method for precipitation events was proposed. The PWV time series retrieved from the Global Positioning System (GPS) observations was processed by using a least-squares fitting method, so as to obtain the line tendency of ascents and descents over PWV. The increment of PWV for a short time (two to six hours) and PWV slope for a longer time (a few hours to more than ten hours) during the PWV ascending period are considered as predictive factors with which to forecast the precipitation event. The numerical results show that about 80%–90% of precipitation events and more than 90% of heavy rain events can be forecasted two to six hours in advance of the precipitation event based on the proposed method. 5-minute PWV data derived from GPS observations based on real-time precise point positioning (RT-PPP) were used for the typhoon event that passed over Zhejiang Province between 10 and 12 July, 2015. A good result was acquired using the proposed method and about 74% of precipitation events were predicted at some ten to thirty minutes earlier than their onset with a false alarm rate of 18%. This study shows that the GPS-based PWV was promising for short-term and now-casting precipitation forecasting.

1. Introduction

The water vapour content in the low atmosphere cycle is one of the most important parameters for water vapour monitoring and precipitation forecasting, but its rapid rate of change makes it difficult to monitor (Li et al., 2012); however, sufficient water vapour content is a prerequisite for any precipitation event. A large-scale and successive or concentrative precipitation event would lead to flooding, with risk to lives and livelihoods. In addition, precipitation is also one of the most important water sources for many regions. Therefore, a short-term precipitation monitoring and forecasting service, especially for high-intensity rainfall, is of vital significance for reducing risk to life and property, and increasing the utilisation of water resources (Chiang et al., 2009).

Traditional water vapour observation methods cannot be applied to the monitoring and forecasting of precipitation events owing to the limitations of their tempo-spatial resolution. For example, the distance between adjacent radiosonde stations is about 200–300 km, and the sounding balloon is launched two or four times per day: such spatial and temporal resolutions are not enough for the monitoring and forecasting needed at the meso- or small-scales. Microwave radiometers are very expensive and cannot work on rainy days, so, their use is not extensive in practice (Bevis et al., 1994; Baker et al., 2001). Since Bevis et al. (1992) proposed the concept of GPS meteorology, ground-based GNSS has gradually become one of the most important means with which to acquire the integrated water vapour (IWV) data and analyse precipitation events. The Global Navigation Satellite System (GNSS) has undergone more than twenty years' development, many cities have established their own Continuously Operating Reference Station (CORS) networks. For instance, there are more than five thousand continuously operating ground-based GNSS stations evenly distributed across each province of China, which is sufficient to meet the requirement for water vapour analysis at meso- and small-scales.

Currently, GNSS-based PWV is mainly derived from two techniques, one is the precise point positioning (PPP) technique based on non-differenced observation; the other is the baseline or network

* Corresponding author.
E-mail address: zhaoqingzhia@163.com (Q. Zhao).

https://doi.org/10.1016/j.jastp.2017.11.013
Received 19 July 2017; Received in revised form 3 November 2017; Accepted 22 November 2017
Available online 23 November 2017

calculation based on double-differenced observations (Zumberge et al., 1997; Dow et al., 2009; Caissy et al., 2012). Compared to the latter, the PPP technique can be used without introducing the assisted station with a baseline longer than 500 km, the resolution of a single station based on the PPP technique is both effective and time-efficient. A series of studies have shown that, whether it is based on non-differenced or double-differenced observations, the accuracy of PWV derived from GPS are comparable in precision with classical measurements from water vapour radiometers, radiosondes, or radar (Bevis et al., 1992; Rocken et al., 1995; Seco et al., 2012; Ortiz de Galisteo et al., 2014). Li et al. (2012) used ZTD, and increments therein, for the rainstorm now-casting. Benevides et al. (2015) proposed a simple algorithm with which to forecast rain in the 6 h after a significant increase in the GPS PWV at a single station.

The aim of this study is to analyse the PWV derived from the PPP technique using GPS data and relevant precipitation information, so as to explore the relationship between PWV and precipitation and provide useful information for short-term, real-time forecasting. One full year of hourly precipitation data for the experimental precipitation stations were accumulated and hourly PWV data for relevant GPS stations were processed in Zhejiang Province, China using the developed PPP software. According to the correlation between PWV and precipitation events, a novel precipitation forecasting model was proposed and also was tested using data derived from other areas. The proposed model was also used for a typhoon event based on the PWV time series derived from the RT-PPP.

2. GPS observation processing

The data-processing software used for GNSS observations includes GAMIT/GOBK and Bernese GNSS Software V5.2, which all provide the zenith troposphere delay (ZTD) above the station with a high accuracy. The ZTD is obtained using the mapping function which projects the slant path delay into the zenith direction at the station, which generally consists of zenith hydrostatic delay (ZHD) and zenith wet delay (ZWD). The main contribution to ZTD (about 90% of ZTD at sea level), which is determined by the altitude and surface pressure of the station, is called ZHD, and can be obtained precisely using the empirical model. Another contribution is ZWD (about 2–20% of ZTD), which takes place at different signal frequencies and is mainly influenced by the dipolar moment of water vapour molecules that lead to a delay in signal propagation. In addition, a few hours before the precipitation event, the signal propagation is also affected by the zenith delay of hydrometeors (ZHMD, about 0–3% of ZTD), which exhibits a relative high variability before, and after, precipitation (Solheim et al., 1999; Hajj *et al.*, 2002; Brenot et al., 2006).

ZHD above the station can be calculated precisely using the observed surface pressure based on the Saastamoinen model (Saastamoinen, 1972):

$$ZHD = \frac{0.002277 \cdot P_s}{1 - 0.00266 \cdot \cos(2\varphi) - 0.00028 \cdot H} \quad (1)$$

Where P_s is the surface pressure (unit: hPa), φ is the latitude, and H represents geodetic height (unit: km). ZHD is a function of surface pressure after the station is determined. An increment of 1 hPa surface pressure only causes about 0.2 mm of ZHD error (Tregoning and Herring, 2006).

Usually, an accurate ZWD is extracted from ZTD by subtracting the ZHD, and the PWV is then obtained by conversion from ZWD (Bevis et al., 1994).

$$\mathrm{PWV} = \frac{10^6}{\left(k_2^{'} + \frac{k_3}{T_m}\right) \cdot R_v \cdot \rho} \cdot \mathrm{ZWD} \quad (2)$$

Where, $k_2^{'} = 16.48 K \cdot hPa^{-1}$ and $k_3 = (3.776 \pm 0.014) \times 10^5 K^2 \cdot hPa^{-1}$ are constants, $R_\omega = 461 (J \cdot kg^{-1} \cdot K^{-1})$ represents the ideal gas constant for water vapour, ρ is the density of the water vapour density, T_m is a mean temperature of the atmospheric column. Usually, T_m is calculated using the observed surface temperature based on the empirical model constrained by sufficient radiosonde or reanalysis data (*i.e.* ECMWF data) (Bevis et al., 1994). In our study, the value of T_m is estimated according to the empirical model established for the east of China using a yearly set of radiosondes located in the east of China (20°–50°N, 100°–130°E).

PWV is the total water vapour content of a unit area in the atmospheric column (unit: kg/m^2), which is equal to the liquid water content at the same height (unit: mm), and is related to the integrated wet profile above the station (Benevides et al., 2015). After the ZWD above the station is determined, PWV is only correlated with T_m: an experiment has been implemented by Bevis to validate that the error caused by Eq. (2) is 1%–2% (Bevis et al., 1994). Brenot et al. (2006) also found that the PWV error is less than 0.3 mm (based on Eq. (2)), which is more accurate than the PWV derived from direct meteorological observations.

3. Experimental data and processing

3.1. Introduction and selection of data

Zhejiang Province is located in the eastern coastal region of China, and has a sub-tropical monsoon climate and meteorological disasters often take place such as typhoons, severe rain, droughts, and floods. This area is characterised by its large spatial-temporal variability of water vapour and spatial precipitation heterogeneity, the annual mean precipitation ranges from 980 to 2000 mm and mainly occurs in summer (May to July). In our study, the GPS and meteorological data were collected from a CORS network constituted by 86 grounded-based stations evenly distributed across Zhejiang Province. Hourly precipitation information about typhoon CHAN-HOM 1509 was provided by Water Conservancy Bureau of Zhejiang. In addition, one GNSS station with meteorological data and one precipitation station in Wuhan City, Hubei Province were also selected (data provided by International GNSS Service (IGS) and Wuhan Municipal Water Affairs Bureau, respectively).

As for obtaining the PWV data, GPS observations were processed by using the newly-developed PPP software, and then accurate PWV data were obtained by combining the observed meteorological data. In spite of the dense GNSS station coverage in Zhejiang Province, unfortunately, the ground-based GPS stations around radiosonde 58457 (green rectangle, Fig. 1(b)) are not equipped with meteorological sensors, so an accurate PWV measure is unavailable. Therefore, one radiosonde (station 45004) and the corresponding GPS station HKSC in the Hong Kong Satellite Positioning Reference Station Network (SatRef) are selected to compare the accuracy of PWV derived from the developed PPP software, as shown by the green rectangle and black triangle in Fig. 1(a), respectively.

Fig. 1 illustrates the geographical distribution of the GNSS stations (black triangles), jointly with the tracking path of typhoon CHAN-HOM 1509 and it also gives the location of the radiosonde station (green rectangles) as well as the collocated precipitation station (red circles) used in our study. Six GPS stations with the nearby precipitation stations were selected for revealing the relationship between PWV and precipitation, in which the elevations vary from 28 m at WUHN to 170 m at ZJXC. The 5-minutely PWV of three GNSS stations (JIAX, ZHOS, and YYAO) were considered for this forecast of real-time precipitation, based on the RT-PPP, during a typhoon event from 10 to 12 July, 2015.

3.2. Accuracy analysis of PPP ZTD

It is reported that the internal accuracy of ZTD derived from PPP module in Bernese GNSS Software (v5.2) reaches ± 1.3 mm, with the mean bias being less than 7 mm (Kyoung Min, 2014; Wilgan, 2015). In addition, the external accuracy of estimated ZTD parameter by GAMIT

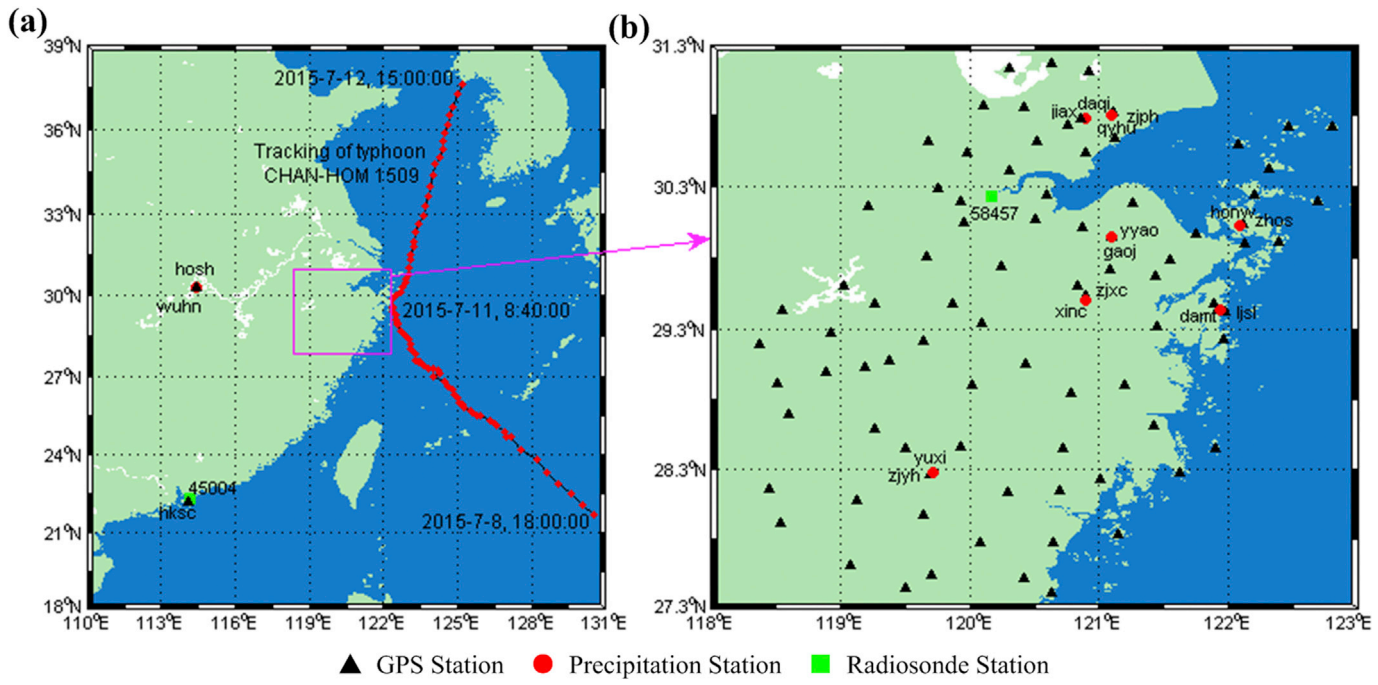

Fig. 1. Location of GNSS, radiosonde and precipitation stations used.

(v10.5) is superior to ± 10 mm (Gusfarienza et al., 2015). Therefore, the results from both Bernese GNSS Software and GAMIT/GLOBK are regarded as the reference against which to investigate the result derived from this PPP software. The propagated paths of signals received by different stations are similar owing to the short baselines between stations in a local area when the GPS observations are processed by GAMIT software based on the double-differenced model. Consequently, the strong correlation of the signal delay caused above the atmosphere among stations is present and the ZTD and PWV derived from such a case are relative values. In our study, the correlation between tropospheric parameters across the network was reduced by introducing three IGS station (BJFS, LHAZ, and SHAO) with the length of baseline therein being greater than 500 km (Rocken et al., 1995).

Bernese GNSS software V5.2 (Dach et al., 2015) and GAMIT/GOBK software V10.5 (Herring et al., 2010) were both used for data processing with a sampling interval of 30 s. Here, BSW and GMT are the abbreviation denoting the Bernese GNSS Software and GAMIT/GLOBK. The time period, of processed data, ran from 1 to 31 May, 2015 with seven GNSS stations in Zhejiang Province. The parameters of ZTD and horizontal variation gradients are estimated within a time interval of 0.5 h and 2 h,

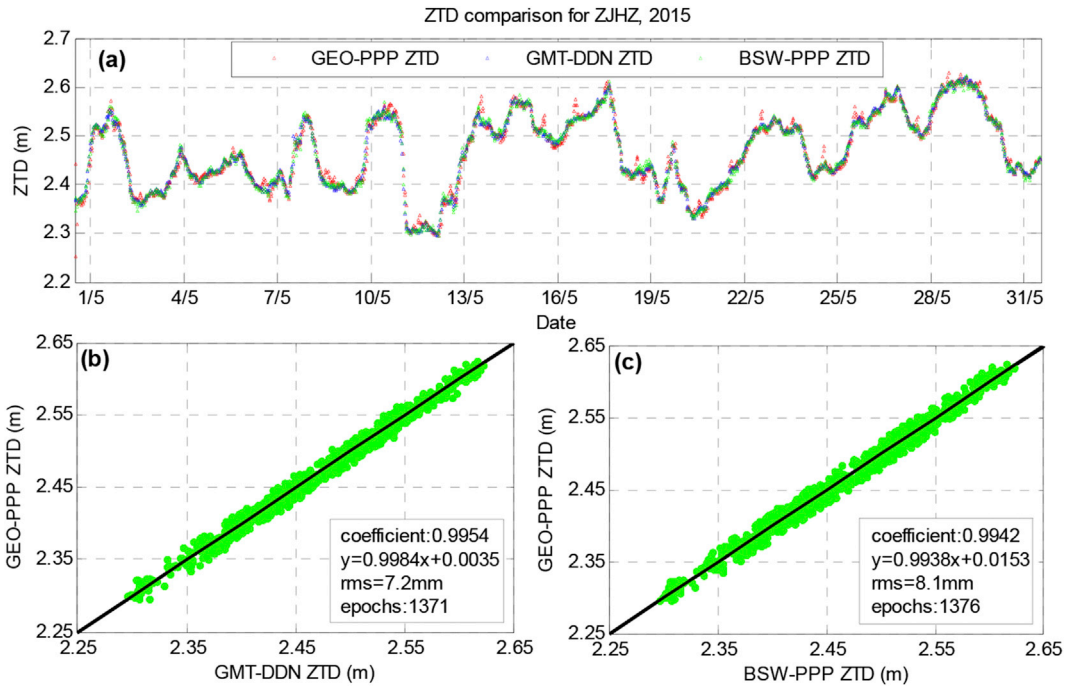

Fig. 2. Comparison of ZTD from GEO-PPP, BSW-PPP and GMT-DDN for ZJHZ for May 2015. (a) ZTD time series, (b) correlation plot of ZTD from GEO-PPP and GMT-DDN and (c) correlation plot of ZTD from GEO-PPP and BSW-PPP.

respectively. An elevation angle mask of 10° is selected and the projection of the slant path delay to the station zenith position based on the Global Mapping Function (GMF) (Böhm et al., 2006) is applied. Here, GEO-PPP refers to that PPP software developed by the College of Geomatics, BSW-PPP denotes PPP with BSW, and GMT-DDN refers to the double-differenced network solutions with GMT. Fig. 2 shows the comparison of ZTD derived from the GEO-PPP, BSW-PPP and GMT-DDN at station ZJHZ. It is clearly shown that the series of ZTD derived from GEO-PPP has a good consistency with that from BSW-PPP and GMT-DDN. According to the statistical analysis of the experimental data, the RMS and coefficient of ZTD are 7.2 mm and 0.9954 compared to that from GMT-DDN, and 8.1 mm and 0.9942 compared to that from BSW-PPP, which evinced the accuracy of ZTD derived from the GEO-PPP as being high enough for meteorological application.

3.3. Accuracy analysis of PPP PWV

Radiosonde data can provide accurate water vapour density profile information (Niell et al., 2001; Adeyemi and Joerg, 2012; Liu et al., 2013), and PWV data with high precision could be obtained by integrating the water vapour plot in the vertical direction; however, as mentioned above, GNSS stations near the radiosonde station in Zhejiang Province do not possess coupled meteorological station sensors, and as a consequence, accurate PWV data were not available for these stations. Fortunately, one radiosonde (station 45004) and a ground-based GPS station HKSC equipped with meteorological sensors are available in Hong Kong (Fig. 1(a)), and the radiosonde data, GNSS observation and meteorological data for two years from 2013 to 2014 were selected so as to validate the accuracy of PWV data derived from the GEO-PPP. Using the processing strategy mentioned above, PWV was calculated by introducing accurate meteorological measurements from the ground-based GPS station using the GEO-PPP and comparisons with radiosonde data-derived PVW (RS PWV). The comparison of the PWV time series at UTC 00:00 and 12:00 (daily) derived from the developed PPP software and radiosonde is shown in Fig. 3. The PWV time series from this PPP software and radiosonde agree with each other. According to the analysis of this test data, the correlation coefficient is 0.9937, and the RMS and bias of the PWV differences are 2.19 mm and 1.17 mm, respectively (Fig. 3(b)), which is the same as the accuracy published by international counterparts (Ortiz de Galisteo et al., 2014; Benevides et al., 2015).

4. The relationship between PWV and precipitation

To analyse the correlation between PWV and precipitation, four GPS stations (ZHOS, LJSL, ZJXC, and ZJPH) and relative precipitation stations (HONW, DAMT, XINC, and QYHU) in Zhejiang Province for one full year (1 September, 2014 to 31 August, 2015) were selected. Four selected GPS stations were all equipped with meteorological sensors and the distance from the closest precipitation event is less than 4 km (see Fig. 1). Hourly PWV data for four stations were retrieved from the GPS observations and meteorological data based on the developed PPP software, and hourly precipitation for the corresponding precipitation stations was accumulated.

The variability of PWV has a clear annual cycle and is related to the local climate (Jin et al., 2007; Byun and Bar-Sever; 2009). Fig. 4 illustrates the time series of hourly PWV variability and hourly precipitation at ZJXC. By calculation, we found that the hourly PWV value ranges from 20 mm in winter and up to about 60 mm in summer. Monthly mean precipitation is about 30 mm in winter but up to 120 mm in summer. This is clear evidence that the strong synoptic variability is relevant to the water vapour carried by meteorological systems.

Hourly PWV data from ZJXC and ZJPH (Zhejiang Province) were selected on 8 March to 6 April, 2015 and 24 May to 22 June, 2015, respectively, so as to reflect the trend in any change in PWV with time. Relative hourly precipitation at XINC and QYHU was considered, to embody the relationship between precipitation and time. Fig. 5(a) and (b) show the time series of PWV and precipitation at ZJXC and ZJPH, respectively.

It can be seen from Fig. 5 that, in cases with significant precipitation, the evolution of PWV follows a typical pattern that may help in forecasting. PWV variations increase gradually before precipitation because precipitation needs a sufficient water vapour supply, which results in a continuous increase in the amount of water vapour in atmosphere in the few hours, or even more than ten hours, before precipitation, so the amount of PWV increases, and the increasing trend of PWV is embodied. Several studies have been shown that precipitation occurred when the PWV reaches its peak or the initial period of its sharp decrease (Li et al., 2012; Benevides et al., 2015); however, not all increasing PWV values would lead to precipitation, just as shown by Fig. 5(b) that the PWV variation had a clear rising trend from 12 June to 15 June, 2015 for ZJXC, but no precipitation occurred then. The two main reasons for this may be that: (1) the monitoring region of the precipitation station is limited, and (2) the advection of water vapour, which leads to some precipitation events not being monitored, as the rain fell elsewhere. In addition, the hourly increment of PWV and hourly precipitation was shown in Fig. 6: some large increments in PWV before precipitation are found. According to the statistical analysis of the experimental data, the precipitation happened after increments of PWV exceeded 2.5 mm/h in the two to six hours earlier, and after precipitation, the increments of PWV would exceed −2.5 mm/h once again.

To study further the specific correlation between GPS PWV and precipitation event, hourly PWV for four ground-based GNSS stations (ZHOS, ZJXC, LJSL, and ZJPH) and the hourly precipitation for collocated precipitation stations for the periods from 5 May to 17 May, 6 June to 25 June, 11 June to 30 June, and 9 March to 28 March, 2015 were selected (Fig. 7), respectively. It can be seen from Fig. 7 that the PWV series is not only continuous and increasing before precipitation (red ovals, Fig. 7), but also exhibits a various significant increment in the two

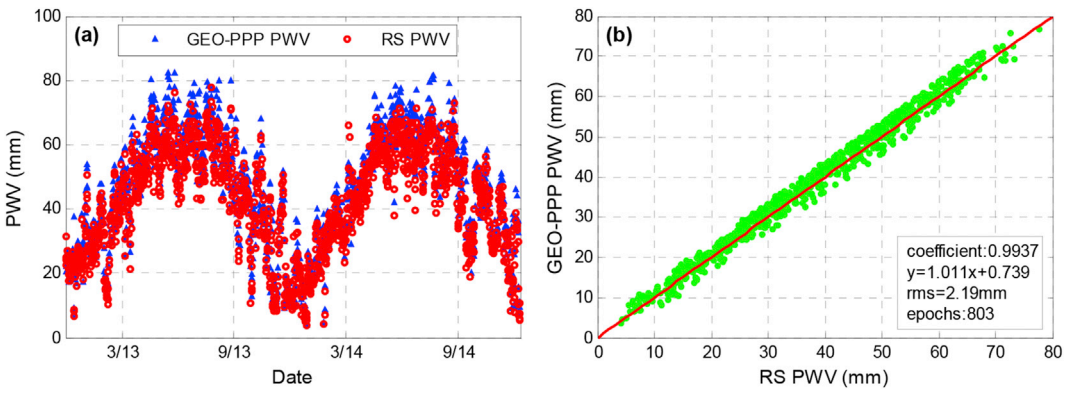

Fig. 3. Comparing PWV derived from GEO-PPP with that from radiosonde data in HKSC at date 2013–2014.

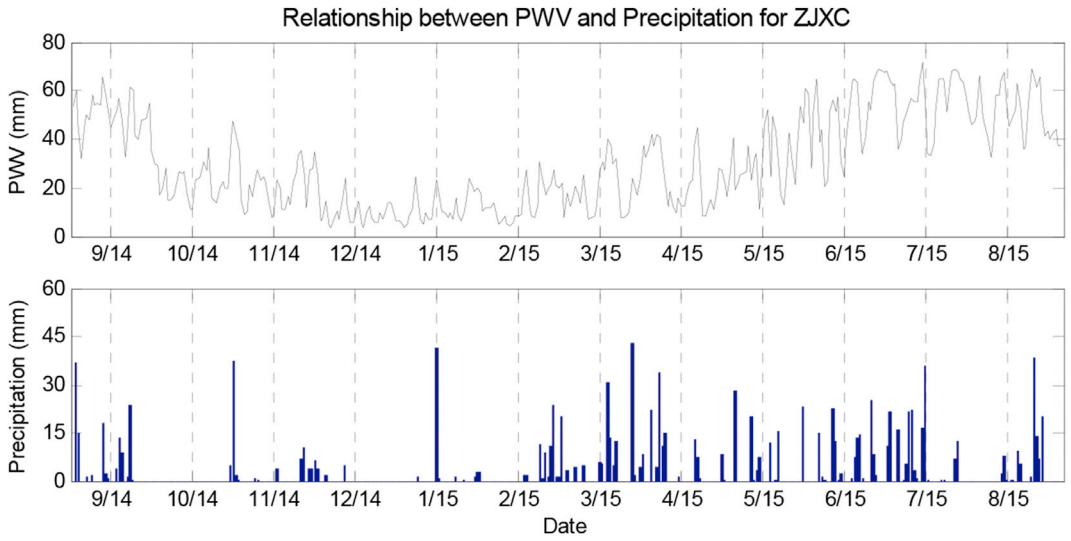

Fig. 4. PWV continuous yearly series at station ZJXC (top panel). Daily accumulated precipitation at station XINC is provided in blue (bottom panel). (For interpretation of the references to colour in this figure legend, the reader is referred to the web version of this article.)

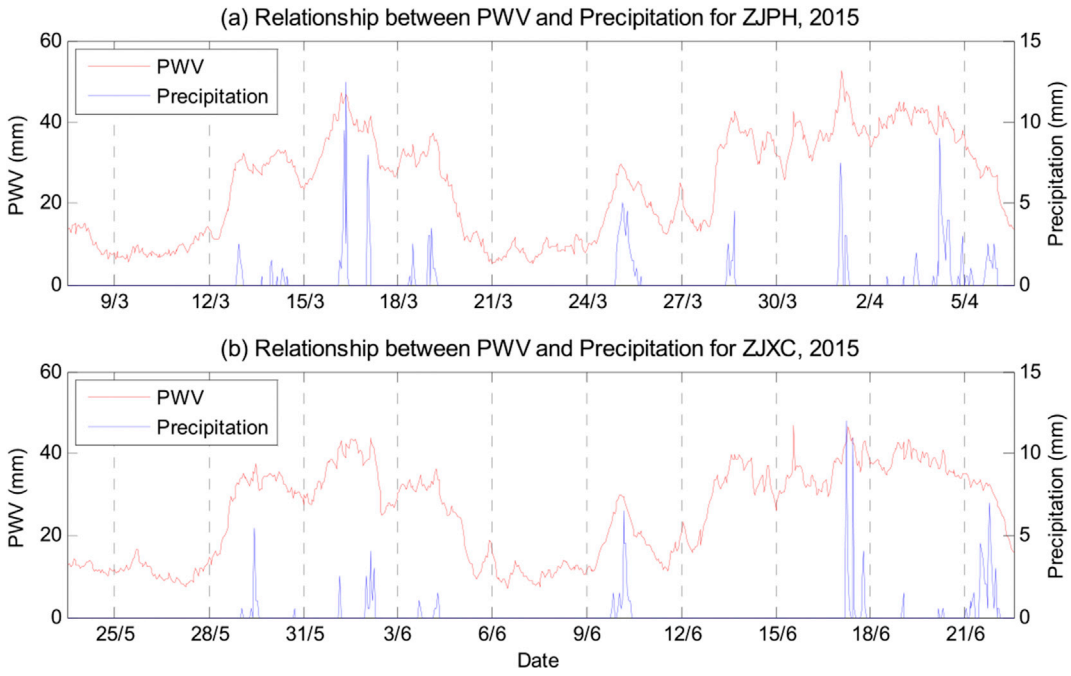

Fig. 5. Time series of hourly PWV and accumulated precipitation for (a) ZJPH for 8 March 2015–6 April 2015 and (b) ZJXC for 24 May 2015–22 June 2015.

to six hours before precipitation (Table 1). The increment of PWV is very large during a short period of two to four hours, and the largest increment of PWV can reach 24.4 mm in four hours while the smallest increment also reaches 2.1 mm in one hour.

The reason for the sharp increment of PWV before precipitation is mainly affected by ZHMD. It has been shown that satellite signals will suffer from the influence of hydrometeors before precipitation, which leads to the delay in signal propagation. A hydrometeor consists of liquid water and icy hydrometeors, usually the contributions induced by liquid water hydrometeors are ten times larger than those of icy hydrometeors (Brenot et al., 2006). The convergence and concentration of water vapour a few hours before precipitation would generate hydrometeors, which contribute to the rapid increase of ZHMD (the maximum is about 7 cm), and are demonstrated by the sharp increase in PWV. Li et al. (2012) have found that the PWV increases some two to six hours before precipitation, and PWV and precipitation present a good positive correlation with respect to the length of time. One point that should be noted is that the changes in PWV are not smooth, and some slight fluctuations are caused by external dynamic factors, however, the similar trend is validated in that PWV increases before precipitation, and decreases after precipitation.

5. GPS-based PWV for precipitation forecasting

5.1. Feasibility analysis

The analysis of hourly PWV and collocated precipitation has proved that the increment of PWV is very large in the two to six hours before precipitation, and the maximum value is greater than 20 mm while the minimum value is also over 2 mm. In addition, PWV has a continuous

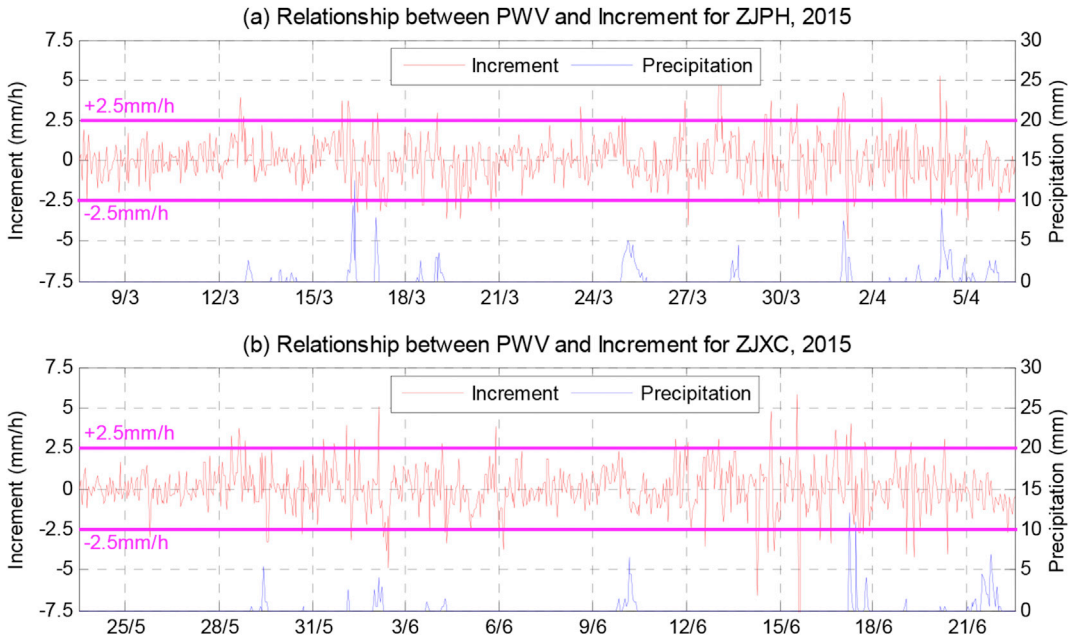

Fig. 6. Time series of hourly PWV increment and accumulated precipitation for (a) ZJPH for 8 March 2015–6 April 2015 and (b) ZJXC for 24 May 2015–22 June 2015.

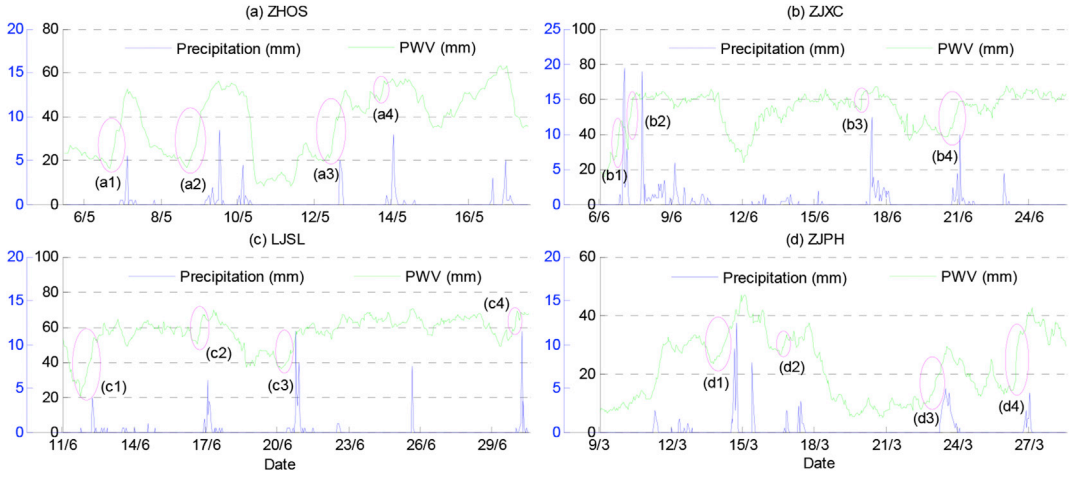

Fig. 7. Time series of hourly PWV and accumulated precipitation for (a) ZHOS for 6 May 2015–17 May 2015, (b) ZJXC for 6 June 2015–25 June 2015, (c) LJSL for 11 June 2015–30 June 2015 and (d) ZJPH 9 March 2015–28 March 2015.

Table 1
Statistical result of PWV increment in a few hours before precipitation for four stations.

Precipitation events	PWV increment(mm)	Time period (h)	Precipitation events	PWV increment(mm)	Time period (h)
(a1)	11.3	3	(c1)	13	4
(a2)	13.7	4	(c2)	8.5	2
(a3)	15.9	3	(c3)	6.6	2
(a4)	9.1	3	(c4)	10.7	3
(b1)	17.6	4	(d1)	3.5	2
(b2)	26.4	4	(d2)	2.1	1
(b3)	8.2	2	(d3)	2.9	1
(b4)	8.4	4	(d4)	15.4	4

increasing period which would last for a few hours, to more than ten hours, before precipitation. Therefore, the maximum increment in PWV occurs within four hours and the PWV slope, during its growth, are two predictive factors used in precipitation forecasting. One point should be noted that the longer-term PWV slope often refers to the few hours, to more than ten hours, before rain. More than 90% of the PWV slope occurs in the period two to sixteen hours ahead of rain.

The feasibility of two factors mentioned above for precipitation forecasting was first verified, and a full year of hourly GPS PWV and collocated precipitation for ZJXC station were analysed. The trend of ascending and descending of PWV was obtained by using least-squares fitting method, and then compared to the hourly precipitation of collocated precipitation stations. Table 2 lists the forecast relationship between the maximum increment of PWV in four hours and the

Table 2
Relationship between PWV increment and the number of precipitation events.

Threshold (mm)	[0 1]	[1 3]	[3 6]	[6 10]	>10	Total
Precipitation times	12	101	59	25	11	208
PWV increment	311	982	421	107	26	1847
Percentage (%)	3.86	10.23	14.01	23.36	42.31	11.26

Table 3
Relationship between PWV slope and the number of precipitation events.

Threshold (mm/h)	[0 0.2]	[0.2 0.5]	[0.5 0.9]	[0.9 1.4]	[1.4 2]	>2	Total
Precipitation times	16	37	66	59	35	30	243
PWV slope	649	983	799	435	164	101	3131
Percentage (%)	2.47	3.76	8.26	13.56	21.34	29.7	7.76

precipitation events during the continuous PWV growth period. Table 3 displays the correlated relationship between PWV slope and precipitation events during the continuous PWV growth period.

The statistical results (Tables 2 and 3) have shown that the percentage of forecast precipitation events increased with increasing threshold of the increment of PWV and PWV slope. Only 3.86% of precipitation events can be forecast when the range of PWV increment is [0 1 mm], and about 23.36% of precipitation events could be forecast when the increment in PWV increased to [6 mm, 10 mm]. Only 2.47% of precipitation events can be forecast when the PWV slope is [0, 0.2 mm/h], and about 22.34% could be forecast at PWV slopes of [1.4 mm/h, 2 mm/h]. There are 259 precipitation events in ZJXC in one year, and 80.30% of precipitation events (208 events in 259) are forecast based on the increment of PWV as a forecasting factor, while 93.82% of precipitation events (243 events in 259) are forecast based on PWV slope data. The average value of precipitation events for the collocated precipitation station ZJXC is 5.81 mm, and the well forecast mean precipitation event is 6.77 mm while the mean of missed precipitation events is 2.82 mm based on the increment of PWV. The average value of forecast precipitation events is 5.99 mm while the average value of missed precipitation events is 3.19 mm based on the PWV slope. The results show that most precipitation events with large rainfall would be well forecast based on the increment of PWV and PWV slope, therefore, the selection of these two factors is deemed feasible.

5.2. Selection of the threshold

Here, some terms are first defined in order to express the relationship between PWV and precipitation events. The term of well-forecast precipitation events (Q) refers to the actual precipitation event, which can be forecast based on the method proposed in this paper. The term of the total forecast precipitation events (M) denotes the total number of precipitation events forecast based on the proposed method, including both real and false precipitation events. The term N refers to the actual total number of precipitation events. Therefore, the success rate and false rate of precipitation forecasting can be expressed as a percentage success rate given by $100Q/N$ while the false forecast rate (as a percentage) is given by $100(M - Q)/M$.

Although a large value of the percentage of precipitation events can be forecast while the threshold is higher, in fact, the number of precipitation events that are well-forecasted is decreasing (the higher the threshold, the lower the number of precipitation event). So, how to select a reasonable threshold from the given range is a key issue. According to the purpose of precipitation forecasting, the thresholds of PWV increment and PWV slope should follow the principle that guaranteeing the maximally well-forecast precipitation events while reducing the false alarms is essential. Here, a full year of hourly PWV data for ZJXC was used as an example for the selection of thresholds. The influences on the percentage of well-forecast precipitation events, false alarms, and the average value of well-forecast precipitation events for different selections of thresholds for the increment of PWV and the PWV slope are demonstrated in Fig. 8.

The range of PWV increment is 0.5 mm–3 mm and the selected interval is 0.5 mm (Fig. 8(a)), while the range of PWV slope is 0.2 mm/h to 1.2 mm/h and the selected interval is 0.2 mm/h. Fig. 8 shows that, with the increasing of thresholds of PWV increment and PWV slope, the percentage of well-forecast precipitation events (including precipitation larger than 0 mm and 15 mm) and the number of false alarms show a downtrend, the case of decreasing trend in precipitation over 0 mm is obvious and for precipitation over 15 mm followed, the downtrend of false alarms is shallow. The average precipitation events that are well-forecast increased (Fig. 8(a)) while the average value of well-forecasted precipitation rose at first and then fell (Fig. 8(b)). When the thresholds of PWV increment and PWV slope at [0.7 mm, 1.2 mm] and [0.3 mm/h, 0.5 mm/h] are selected, respectively, the percentage of well-forecast precipitation events (including precipitation larger than 0 and 15 mm) is higher, and the false alarm rate decreases: the average value of well-forecast precipitation events increases, therefore, 1 mm and 0.4 mm/h are determined as optimal thresholds for PWV increment and PWV slope at ZJXC.

5.3. Validation of GPS PWV precipitation forecasting

The experiment of GPS PWV precipitation forecasting was implemented based on the thresholds determined above. Among the 259 precipitation events for a full year at ZJXC, 214 precipitation events can be forecast within two to six hours of precipitation, in addition, 20 heavy precipitation events can be found in the total of 22 rain events based on

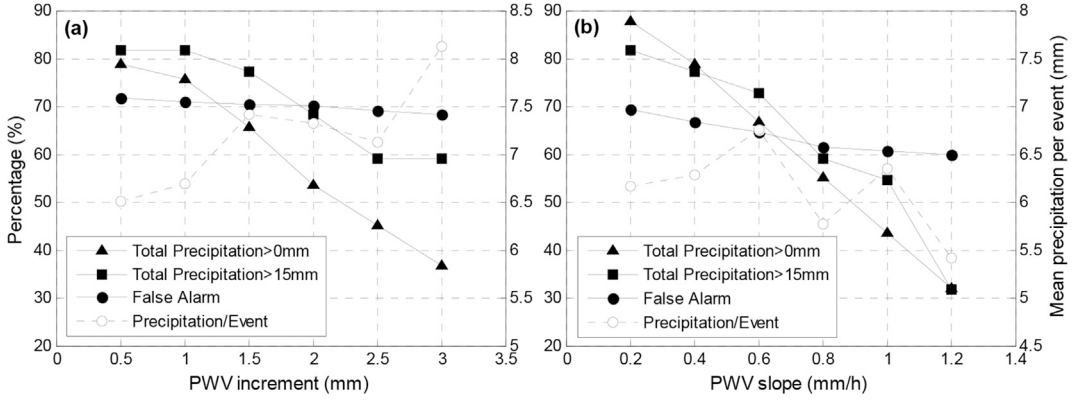

Fig. 8. Relationship between thresholds of (a) PWV increment and (b) PWV slope, and percentage of forecasted events, false alarms and mean accumulated rain in the well forecasted events.

Table 4
Thresholds and statistical result of forecasted precipitation events for different stations.

Station	PWV increment (mm)	PWV slope (mm/h)	True>0 mm (%)	True>15 mm (%)	False alarm (%)
LJSL	2	0.6	80.18(172/222)	96 (24/25)	69.15
ZHOS	2	0.8	84.47(172/206)	100(10/10)	68.36
ZJPH	1	0.6	86.5(199/230)	91.82(18/22)	69.66
ZJYH	1	0.4	86.20(256/297)	96.97(32/33)	63.17
WUHN	0.1	0.05	87.10(216/248)	94.87(37/39)	60.51
Mean	–	–	84.89	95.93	66.10

the proposed forecasting method, with correct forecasting rates of 87.23% and 90.91%, respectively. Unfortunately, the false forecasting rate is 66.81%.

On the one hand, hourly PWV from four ground-based GNSS stations (LJSL, ZHOS, ZJPH, and ZJYH) was selected in Zhejiang Province for the period 1 September, 2014 to 31 August, 2015 to validate the proposed method. On the other hand, hourly PWV of one ground-based GPS station (WUHN) was also considered in Hubei Province for the full year 2010 with the distance to ZJXC being larger than 600 km so as to verify the universality of the precipitation forecasting method. The thresholds of PWV increment and PWV slope for different stations were first determined based on the method mentioned above, and then the statistical result of forecast precipitation events and false alarms was achieved (Table 4).

It can be seen from Table 4 that the correct rates for cases of precipitation larger than 0 mm at LJSL, ZHOS, ZJPH, ZJYH, and WUHN are 80.18%, 84.47%, 86.52%, 86.20%, and 87.10%, respectively, and the correct rates for cases of precipitation larger than 15 mm are 96%, 100%, 91.82%, 96.97%, and 94.87%, respectively, while the false forecast rates are 69.15%, 68.36%, 69.66%, 63.17%, and 60.51%, respectively. The average correct rates for the cases of precipitation larger than 0 and 15 mm are 84.89% and 95.93%, respectively, while the average false rate is 66.10%. Compared to the forecast method based on GPS-derived PWV published by international counterparts with a correct forecast rate of about 75%, the proposed method has increased the correct rate by about 10%, while the false rate is the same as before (60%–70%) (Benevides et al., 2015). This result shows that the proposed method for precipitation forecasting was effective and universal. Some information also can be found from Table 4 to the effect that the thresholds of PWV increment and PWV slope are similar for LJSL, ZHOS, ZJPH, and ZJYH in Zhejiang Province, while the threshold for WUHN with a distance to ZJXC exceeding 600 km is only about one-tenth of that selected from Zhejiang Province. By comparing the relationship between PWV and the average precipitation (Table 5), we found that the average PWV and average precipitation of five stations in Zhejiang Province for full year are similar, while the differences between maximum and minimum PWV are large compared to that of WUHN, Hubei Province. The maximum PWV at WUHN is 45.07 mm while the minimum is 35.44 mm, which shows a slow rate of change in the trend. The difference between maximum and minimum PWV is 9.63 mm, which is far less than that at stations in Zhejiang Province with a difference of more than 70 mm. Therefore, it is reasonable that lower thresholds were selected at WUHN.

Table 5
Statistical result of PWV and mean precipitation for different stations.

Station	Ave. PWV (mm)	Min. PWV (mm)	Max. PWV (mm)	Dif. PWV (mm)	Precipitation/event (mm)
ZJXC	31.62	1.12	72.76	71.64	18.75
LJSL	32.23	0.43	80.66	80.23	20.49
ZHOS	33.08	0.90	84.12	83.22	17.74
ZJPH	30.24	0.65	78.21	77.56	12.16
ZJYH	35.20	1.53	75.63	74.10	13.83
WUHN	39.08	35.44	45.07	9.63	12.55

5.4. Analysis of precipitation forecasting during a typhoon event

With the development of IGS Real-time Pilot Project (RTPP), PWV derived from the RT-PPP has become a reality with an accuracy of 1.5 mm–2.5 mm (Caissy et al., 2012; Li et al., 2014; Lu et al., 2015; Ahmed et al., 2016). To verify the validity of the proposed method, 5-min PWV derived from RT-PPP was used for precipitation forecasting some ten to thirty minutes earlier. A typhoon event (CHAN-HOM 1509) passed over Zhejiang Province: PWV data at high temporal resolution were obtained based on the RT-PPP for short-term forecasting.

The GPS observations and meteorological data were selected for three stations (ZHOS, YYAO, and JIAX) during the period from 10 to 12 July, 2015. The real-time clock and orbit information with intervals of 10 s and 30 s could be obtained on-line, and the 5-min PWV was calculated based on the RT-PPP. The precipitation forecasting experiment was carried out with the real-time 5-min PWV and was validated by the cumulative 5-min precipitation at collocated stations.

The ZTD and PWV derived from the RT-PPP were first validated. In our study, 5-min ZTD and 5-min PWV derived from PPP technique using real-time, final orbit, and clock products were calculated at ZJHZ during the period from 28 May to 6 June, 2015. Fig. 9 illustrates a scatter plot of ZTD and PWV derived from different methods. The interval of resampled ZTD and PWV is5 minutes, so 2880 ZTD and PWV pairs were obtained during the experimental period. Among all those experimental data, some data are apparently faulty, thus an exclusion rule rejecting incorrect ZTD/PWV pairs was required. In our study, the mean and RMS error were first calculated for the differences between the two ZTD/PWV time series, and then, the final sampling was selected with differences less than three-times the RMS errors. Consequently, 2504 ZTD and PWV pairs were selected for analysis. Compared to the PPP-derived ZTD and PWV based on the IGS final products, the correlation coefficient and RMS of RT-PPP derived ZTD and PWV are 0.9945, and 9.5 mm, and 0.9954, and 1.5 mm, respectively. The results demonstrate that the ZTD and PWV time series derived from RT-PPP were consistent with those arising from the post-processed PPP data. Therefore, it satisfies the precision requirement behind monitoring and forecasting of precipitation events based on PWV derived from the RT-PPP.

A typhoon event (CHAN-HOM 1509) passed through Zhejiang Province (10–12 July, 2015), and landfall hit Zhoushan city at 08:40 UTC 11 July, 2015. Fig. 10 shows the 5-min PWV and precipitation at ZHOS and YYAO during the typhoon. It can be seen from Fig. 10 that ZHOS, located in Zhoushan City, with the coming of typhoon, had a rainstorm that started at 12:00, 10 July. Instead of a drop in PWV after severe rain at 18:00, 10 July, it has a continuously increasing trend and exceeds 100 mm. Compared to station ZHOS, YYAO was less affected by this typhoon, but after landfall, and the heavy rain occurred at 6:00, 11 July, The PWV at station YYAO also increased to nearly 80 mm. The main reason for the increased PWV was that the coming of the typhoon brings sufficient water vapour, and only one heavy rain event is not enough for its rapid decrease thereafter. In addition, horizontal advection during the typhoon period transports a large amount of water vapour. As the typhoon moved north, the PWV of two stations fell gradually, but still remained high compared to the average PWV over a full year (about 32 mm).

Real-time 5-min PWV at three stations (ZHOS, YYAO, and JIAX) were used for precipitation forecasting based on the method mentioned above. Table 6 lists the selection of thresholds and the forecast results from different stations: based on the RTPPP-based PWV, 76.25%, 77.89%, and 68.60% of precipitation events can be forecast within ten to thirty minutes earlier at ZHOS, YYAO, and JIAX, respectively. The average correct rate is 74.25% while the false rate was only 18.05%, which is far less than

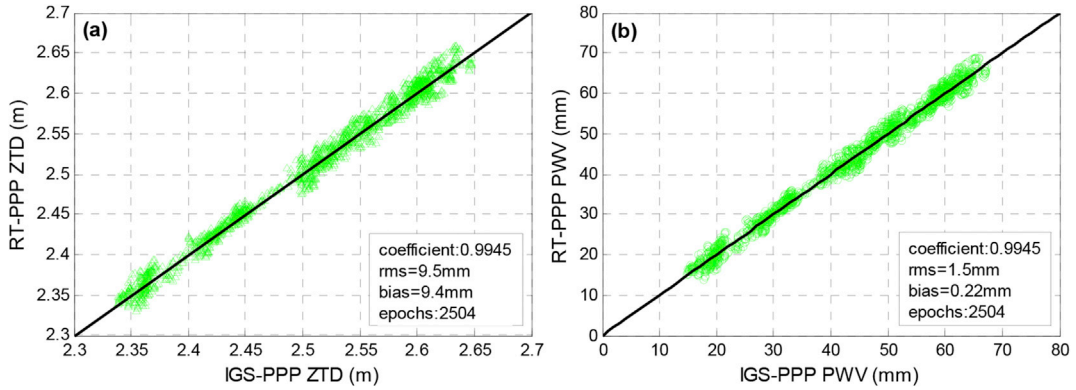

Fig. 9. Correlation plots of ZTD and PWV at ZJHZ station from 28 May to 6 July for (a) RT-PPP ZTD and IGS-PPP ZTD, (b) TR-PPP PWV and IGS-PPP PWV.

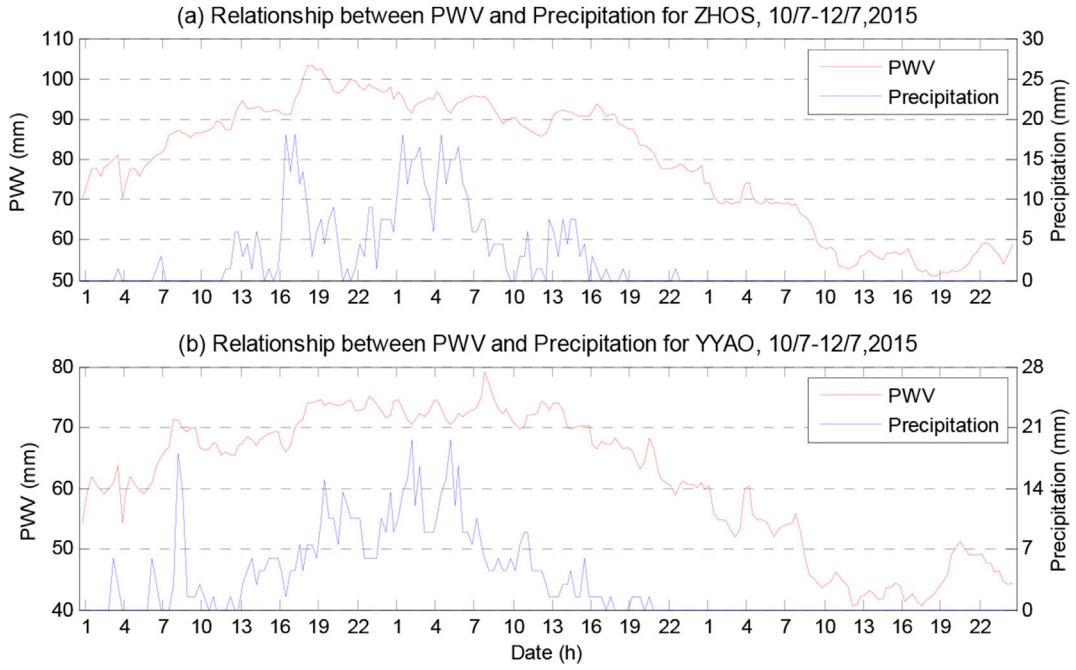

Fig. 10. Relationship between PWV and Precipitation at ZHOS and YYAO stations from 10 to 12 July, 2015.

Table 6
Threshold and statistical result of forecasted rain events for three stations at date from 10 to 12 July, 2015.

Station	PWV increment (mm)	PWV slope (mm/5min)	True (%)	False alarm (%)
ZHOS	0.5	0.2	76.25 (183/240)	26.51
YYAO	0.5	0.2	77.89 (236/303)	9.58
JIAX	0.4	0.2	68.60 (59/86)	18.06
Mean	–	–	74.25	18.05

the false result when using hourly PWV with an average false rate of 66.10%. One reason was that the most precipitation events were heavy rain during this typhoon and the variability of PWV was evident. Another explanation was that the PWV and precipitation with higher temporal resolution were introduced to the problem.

6. Discussion and conclusion

A series of studies by different authors evinces the variability of water vapour content in different precipitation conditions, and demonstrates the existence of a positive correlation between the evolution of PWV and precipitation events; however, some false relevance remained (Champollion et al., 2004; Bastin et al., 2007; Yan et al., 2009; Brenot et al., 2014; Benevides et al., 2015). Some of the evident false correlation between PWV and precipitation may be related to the limitation of monitoring ability of precipitation gauges or the three-dimensional nature of the water vapour field, one-dimensional PWV is the mean projected by the water vapour content of different elevations and azimuths to the zenith point, which is not enough to reflect the three-dimensional variability information about water vapour derived by a single GPS station.

A long-term PWV series retrieved from GPS observation and meteorological data was analysed in our study and compared to the corresponding precipitation events. The result shows that the precipitation occurred at peak PWV and the initial period of its rapid decrease thereafter. Based on the findings above, a precipitation forecasting method was proposed using the PWV increment and PWV slope as forecasting factors during the continuously ascending period. Some ground-based GPS stations of the CORS network in Zhejiang Province and WUHN station in Hubei Province, combined with collocated meteorological data and precipitation information were employed to validate the proposed method. The experimental result shows that more than 80% of precipitation events, and more than 90% of heavy precipitation can be forecast up to two to six hours earlier, which manifested the universality and

reliability of the proposed method. Unfortunately, the false forecast rate was 60%–70%. In addition, the present method has the limitation that, in its present form, it does not predict the amount of precipitation, only its occurrence.

The application of the forecasting method was implemented during the typhoon event based on the 5-min PWV retrieved after using the RT-PPP. The result indicates that, despite its extremely active and complicated nature with regards the PWV, 74.25% of precipitation events could be forecast within ten to thirty minutes earlier with a false forecast rate of less than 20%. Compared to the result forecast using hourly PWV, the correct forecast rate using 5-min PWV decreased slightly, but the false alarm rate dropped significantly, which is likely to be attributable to us adopting PWV with a higher temporal resolution. Therefore, decreasing the false forecast rate by improving the temporal resolution of PWV is worthy of future research.

Considering only one-dimensional PWV above a single station was used for precipitation forecasting, if more observations of GPS stations in regional area with meteorological data were included, and we studied the three-dimensional water vapour distribution, the forecast result would be more promising, which also forms a focus for future research. The forecast result can be used for short-term forecasting and increases the ability of imminent predictions, especially for synoptic forecasting. In addition, it is also important for the study of water vapour transportation and the efficient use of the atmospheric water resource.

Acknowledgement

The authors would like to thank IGAR for providing access to the web-based IGAR data. The IGS, Lands Department of HKSAR and Zhejiang Administration of Surveying Mapping and Geo-information are acknowledged for providing GPS experimental data. The Water Conservancy Bureau of Zhejiang province and Water Authorities of Wuhan are also acknowledged for providing precipitation information. This research was supported by the National Key Research and Development Program of China (2016YFB0501803) and the National Natural Science Foundation of China (41574028).

References

Adeyemi, B., Joerg, S., 2012. Analysis of water vapor over Nigeria using radiosonde and satellite data. J. Appl. Meteorol. Climatol. 51, 1855–1866. https://doi.org/10.1175/JAMC-D-11-0119.1.

Ahmed, F., Václavovic, P., Teferle, F.N., Douša, J., Bingley, R., Laurichesse, D., 2016. Comparative analysis of real-time precise point positioning zenith total delay estimates. GPS Solut. 20 (2), 187–199.

Baker, H.C., Dodson, A.H., Penna, N.T., et al., 2001. Ground_Based GPS water vapor estimation: potential for meteorological forecasting [J]. J. Atmos. Sol. Terr. Phys. 63, 1305–1314.

Bastin, S., Champollion, C., Bock, O., Drobinski, P., Masson, F., 2007. Diurnal cycle of water vapor as documented by a dense GPS network in a coastal area during ESCOMPTE IOP2. J. Appl. Meteorol. Climatol. 46 (2), 167–182.

Benevides, P., Catalao, J., Miranda, P.M.A., 2015. On the inclusion of GPS precipitable water vapour in the nowcasting of rainfall. Nat. Hazards Earth Syst. Sci. Discuss. 3, 3861–3895.

Bevis, M., Businger, S., Chiswell, S., Herring, T.A., Anthes, R.A., Rocken, C., Ware, R.H., 1994. GPS meteorology: mapping zenith wet delays onto precipitable water. J. Appl. Meteorol. 33 (3), 379–386.

Bevis, M., Businger, S., Herring, T., Rocken, C., Anthes, R., Ware, R., 1992. GPS meteorology- Remote sensing of atmospheric water vapor using the Global Positioning System. J. Geophys. Res. 97 (D14), 15787–15801.

Böhm, Johannes, et al., 2006. Global Mapping Function (GMF): a new empirical mapping function based on numerical weather model data. Geophys. Res. Lett. 33.7.

Brenot, H., Ducrocq, V., Walpersdorf, A., Champollion, C., Caumont, O., 2006. GPS zenith delay sensitivity evaluated from high-resolution numerical weather prediction simulations of the 8–9 September 2002 flash flood over southeastern France. J. Geophys. Res. Atmos. (1984–2012) 111 (D15).

Brenot, H., Wautelet, G., Warnant, R., Neméghaire, J., Van Roozendael, M., 2014. GNSS meteorology and impact on NRT position. In: European Navigation Conference (ENC) GNSS 2014.

Byun, S.H., Bar-Sever, Y.E., 2009. A new type of troposphere zenith path delay product of the international GNSS service. J. Geodesy 83 (3–4), 1–7.

Caissy, M., Agrotis, L., Weber, G., Hernandez-Pajares, M., Hugentobler, U., 2012. Coming soon: the international GNSS real-time service. GPS World 23 (6), 52–58.

Champollion, C., Masson, F., Van Baelen, J., Walpersdorf, A., Chéry, J., Doerflinger, E., 2004. GPS monitoring of the tropospheric water vapor distribution and variation during the 9 September 2002 torrential precipitation episode in the Cévennes (southern France). JGeophys. Res. Atmos. (1984–2012) 109 (D24).

Chiang, K.W., Peng, W.C., Yeh, Y.H., Chen, K.H., 2009. Study of alternative GPS network meteorological sensors in Taiwan: case studies of the plum rains and typhoon Sinlaku. Sensors 9 (6), 5001–5021.

Dach, R., Lutz, S., Walser, P., Fridez, P., 2015. Bernese GNSS Software Version 5.2. Astronomical Institute, University of Bern, p. 884.

Dow, J.M., Neilan, R.E., Rizos, C., 2009. The international GNSS service in a changing landscape of global navigation satellite systems. J. Geodesy 83 (3–4), 191–198.

Gusfarienza, H., Yuwono, B.D., Awaluddin, M., Susilo, S., 2015. Penentuan zenith troposphere delay and precipitable water vapour menggunakan perangkat lunak GAMIT. J. Geod. Undip 4 (2), 78–86.

Hajj, G.A., Kursinski, E.R., Romans, L.J., Bertiger, W.I., Leroy, S.S., 2002. A technical description of atmospheric sounding by GPS occultation. J. Atmos. Solar-Terrestrial Phys. 64 (4), 451–469.

Herring, T.A., King, R.W., McClusky, S.C., 2010. Documentation of the GAMIT GPS Analysis Software Release 10.4. Department of Earth and Planetary Sciences, Massachusetts Institute of Technology, Cambridge, Massachusetts.

Jin, S., Park, J.U., Cho, J.H., Park, P.H., 2007. Seasonal variability of GPS-derived zenith tropospheric delay (1994–2006) and climate implications. J. Geophys. Res. Atmos. (1984–2012) 112 (D9).

Kyoung Min, R., 2014. Quality assessment of tropospheric delay estimated by precise point positioning in the Korean peninsula. J. Position. Navig., Timing 3 (4), 131–141.

Li, L., Kuang, C.L., Zhu, J.J., et al., 2012. Rainstorm nowcasting based on GPS real-time precise point positioning technology. Chinses J. Geophys 55 (4), 1129–1136. https://doi.org/10.6038/j.issn.0001-5733.2012.04.008 (in Chinese).

Liu, Z.Z., Wong, M.S., Nichol, J., Chan, P.W., 2013. A multi-sensor study of water vapour from radiosonde, MODIS and AERONET: a case study of Hong Kong. Int. J. Climatol. 33, 109–120. https://doi.org/10.1002/joc.3412.

Li, X., Dick, G., Ge, M., Heise, S., Wickert, J., Bender, M., 2014. Real-time gps sensing of atmospheric water vapor: precise point positioning with orbit, clock, and phase delay corrections. Geophys. Res. Lett. 41 (10), 3615–3621.

Lu, C., Li, X., Nilsson, T., Ning, T., Heinkelmann, R., Ge, M., et al., 2015. Real-time retrieval of precipitable water vapor from gps and beidou observations. J. Geodesy 89 (9), 1–14.

Niell, A.E., Coster, A.J., Solheim, F.S., et al., 2001. Comparison of measurements of atmospheric wet delay by radiosonde, water vapor radiometer, GPS, and VLBI. J. Atmos. Ocean. Technol. 18, 830–850.

Ortiz de Galisteo, J.P., Bennouna, Y., Toledano, C., Cachorro, V., Romero, P., Andrés, M.I., Torres, B., 2014. Analysis of the annual cycle of the precipitable water vapour over Spain from 10-year homogenized series of GPS data. Q. J. R. Meteorol. Soc. 140 (679), 397–406.

Rocken, C., Hove, T.V., Johnson, J., Solheim, F., Ware, R., Bevis, M., Businger, S., 1995. GPS/STORM-GPS sensing of atmospheric water vapor for meteorology. J. Atmos. Ocean. Technol. 12 (3), 468–478.

Saastamoinen, J., 1972. Atmospheric Correction for the Troposphere and Stratosphere in Radio Ranging Satellites. The Use of Artificial Satellites for Geodesy, pp. 247–251.

Seco, A., Ramírez, F., Serna, E., Prieto, E., García, R., Moreno, A., Priego, J.E., 2012. Rain pattern analysis and forecast model based on GPS estimated atmospheric water vapor content. Atmos. Environ. 49, 85–93.

Solheim, F.S., Vivekanandan, J., Ware, R.H., Rocken, C., 1999. Propagation delays induced in GPS signals by dry air, water vapor, hydrometeors, and other particulates. J. Geophys. Res. Atmos. (1984–2012) 104 (D8), 9663–9670.

Tregoning, P., Herring, T.A., 2006. Impact of a priori zenith hydrostatic delay errors on GPS estimates of station heights and zenith total delays. Geophys. Res. Lett. 33 (23).

Wilgan, K., 2015. Zenith total delay short-term statistical forecasts for GNSS precise point positioning. Acta Geodyn. Geomater. 12 (4(180)), xx1–xx9.

Yan, X., Ducrocq, V., Poli, P., Hakam, M., Jaubert, G., Walpersdorf, A., 2009. Impact of GPS zenith delay assimilation on convective-scale prediction of Mediterranean heavy rainfall. J. Geophys. Res. Atmos. (1984–2012) 114 (D3).

Zumberge, J.F., Heflin, M.B., Jefferson, D.C., Watkins, M.M., Webb, F.H., 1997. Precise point positioning for the efficient and robust analysis of GPS data from large networks. J. Geophys. Res. Solid Earth (1978–2012) 102 (B3), 5005–5017.